Journal of Aerospace Engineering, Volume 37, Issue 1, January 2024
DOI:10.1061/JAEEEZ.ASENG-5003

Accepted version

ACSE Journal of Aerospace Engineering
DOI: 10.1061/JAEEEZ/ASENG-5003

Active Stall Flutter Suppression for a Revised Leishman/Beddoes Model

Junruoyu Zheng
Shanghai Aircraft Design and Research Institute, 5188 Jinke Road, Shanghai, 201210, China.

Alessandro Pontillo
School of Civil, Aerospace and Mechanical Engineering, Bristol University, BS8 1TL, UK.

Lejun Chen
Dept of Electronic and Electrical Engineering, UCL, London WC1E 6BT, UK.

James F Whidborne
Centre for Aeronautics, Cranfield University, Bedfordshire MK43 OAL, UK.

Abstract

This paper proposes a nonlinear disturbance observer (NDO) based sliding mode control (SMC) method to the problem of stall flutter suppression for a revised Leishman/Beddoes (L/B) model. To capture accurate aerodynamic characteristics whilst reducing the plant model mismatch, the dynamics of the separation point and the shift of the aerodynamic centre are analysed to improve the structure of the L/B model. Based on this revised L/B model, an active flutter suppression problem which includes aerodynamic disturbances and actuator dynamics is addressed. The inclusion of the actuator dynamics means that the aerodynamic disturbance from the flow separation, induced by the revised L/B model, is considered as an 'unmatched' disturbance. To counteract the effect of unmatched disturbances, an NDO-based sliding mode control scheme is applied to suppress stall flutter and to ensure rapid reference tracking performance in both steady and unsteady flow conditions. Simulation results show the improvements of the proposed revised L/B model via a comparative analysis. In addition, the efficacy of the proposed stall flutter suppression scheme is demonstrated.

1 Introduction

Stall flutter is a nonlinear, dynamic aeroelastic instability with self-excited Limit Cycle Oscillations (LCOs) [Li et al., 2016]. Stall flutter LCOs result from the coupling between dynamic stall and wing torsional mode whereby flow periodically detaches from the wing and reattaches [Niel et al., 2017], generally as a result of large incidence angles. The onset of this phenomenon is usually marked by the flutter speed, which is one of the most important criteria for aircraft safety and performance [Sun et al., 2015]. Traditionally, stall flutter is avoided by stiffening the structure, which invokes a weight penalty [Sun et al., 2015, Doggett and Townsend, 1976], but the drive towards more efficient aircraft by reducing weight and increasing wing aspect ratio means that wings are becoming more flexible [Fagley et al., 2015] and are subject to larger deformations. Indeed, with very flexible wings, such as the NASA HALE Helios vehicle [Fagley et al., 2015], the large deformations mean that the incidence angles on the wingtips can be large even when undergoing lateral maneuvers. Consequently aeroelastic instability is of increasing importance and Active Flutter Suppression (AFS) has received much attention [Livne, 2018].

One challenge of AFS control design is the modelling of unsteady aerodynamic loads [Borglund and Kuttenkuler, 2002]. Stall flutter behaviour can be described with an aerodynamic model coupled with an elastic structural model.

A noted case is the Leishman/Beddoes (L/B) model which is used to model unsteady loads for an airfoil undergoing dynamic stall [Leishman and Beddoes, 1989]. However, since the L/B model was originally developed for helicopter blades at Mach numbers higher than 0.3, it requires certain modifications for incompressible cases [Sheng et al., 2006]. Hence a modified L/B model was proposed [Boutet et al., 2020] for both low Reynolds number and low Mach number cases. However, there exist noticeable model-plant mismatches. To capture more accurately the unsteady loads undergoing dynamic stall, a revised L/B model is proposed here and applied to a NACA 0012 airfoil. This model constructs the dynamics of the separation point and the shift of the aerodynamic centre, and is capable of representing large disturbances from the air flow.

Model-based control approaches have been widely used to suppress stall flutter. One of the earliest schemes was applied to an aileron flutter suppression problem and used root locus analysis and an inverse notch filter with a narrow pass band to compensate adverse zero locations inside the frequency range near flutter [Waszak and Srinathkumar, 1995]. $\mathcal{H}_\infty$-based linear parameter varying or gain-scheduled control laws have been developed to increase the critical flutter speed [Borglund and Kuttenkuler, 2002, Theis et al., 2016]. Another, $\mathcal{H}_2$-norm-based, AFS method managed to expand the flutter envelope by 31% [Sun et al., 2015]. An adaptive control method was proposed that asymptotically stabilised both translational and torsional modes in stall flutter via feeding the pitch rate and the vertical speed of foil section back to a time-varying controller [Li et al., 2016]. More recently, AFS solutions have been successfully validated via hardware-in-the-loop tests and flight tests [Luspay et al., 2019, Takarics et al., 2020].

It is well known that sliding mode control (SMC) has inherent robustness against matched uncertainty [Utkin, 1992, Edwards and Spurgeon, 1998]. This robustness property has been exploited to ensure asymptotic and simultaneous convergence of both translational and torsional modes in LCOs [Ramos-Pedroza et al., 2015]. However, dynamic stall was not considered in the work. Furthermore, existing AFS schemes do not include the actuator dynamics. Due to the presence of the actuator dynamics, the aerodynamic disturbance in the AFS problem will be formulated as unmatched disturbance. Actuator dynamics reduce the performance of feedback control; their presence causes the external disturbances to be unmatched. To overcome this, Yang et al. [2013] developed an SMC scheme that is based on a nonlinear disturbance observer (NDO) that can compensate for the unmatched disturbance. This method is the basis for the approach proposed here. Most notably, uncertain linear actuator dynamics are included in the model.

In this paper, two-dimensional wing-section flutter is considered and a time-domain aeroelastic model for the stall flutter analysis and controller design is developed. To capture more accurately the unsteady loads undergoing dynamic stall, a novel modification of the L/B model is proposed and applied for a NACA 0012 airfoil. Numerical simulation and analysis are performed to demonstrate the onset of stall flutter and LCOs. For flutter suppression, an observer-based sliding mode control scheme is proposed to handle unmatched disturbances due to the existence of the actuator dynamics. In this scheme, an NDO is proposed to estimate unmatched disturbances, which is used to construct the sliding surface. The simulation results show that the controller provides fast, stable, and robust closed-loop responses. The main contributions of this paper are to establish a modified L/B nonlinear airfoil model, and to apply an NDO to suppress the stall flutter in the presence of unmatched uncertainty. Compared with the NDO proposed in Yang et al. [2013] in which the observer gains are constant values, a NDO with state dependent observer gains are created in this paper. This structure is well posed for the situation in which the unmatched uncertainty (induced by actuator dynamics in this paper) affect the channels involving the nonlinear functions/dynamics. The application of an NDO-based control for flutter suppression appears to be new.

In the next section, the modelling of the stall flutter is discussed and a formulation of the modified L/B model is derived. The NDO-based control design is described in Section 3 and the closed-loop stability is proven. In Section 4, some comparative results for the proposed aerodynamics model are given, along with simulation results of the closed-loop system. Finally, some conclusions are provided.

2 Modelling of Stall Flutter

A spring-restrained rigid two-dimensional wing section model is shown in Fig. 1. The elevator surface deflection is considered as the control input for pitch and plunge. In the usual manner, two reference frames are contained in the model [Li et al., 2016, Sun et al., 2015, Beedy et al., 2003, Yang et al., 2010, Peiró et al., 2010]. The aerodynamic reference frame has normal force, N, positive upwards and perpendicular to the chord line and pitch moment, M, positive nose-up; these act at the aerodynamic centre point (AC). Under attached flow conditions, AC is assumed to be located at the quarter chord, the half-chord is denoted by b. The kinematic frame has plunge distance, z, positive downwards measured at the elastic axis origin (EA). The dimensionless parameter a denotes the relative distance of the

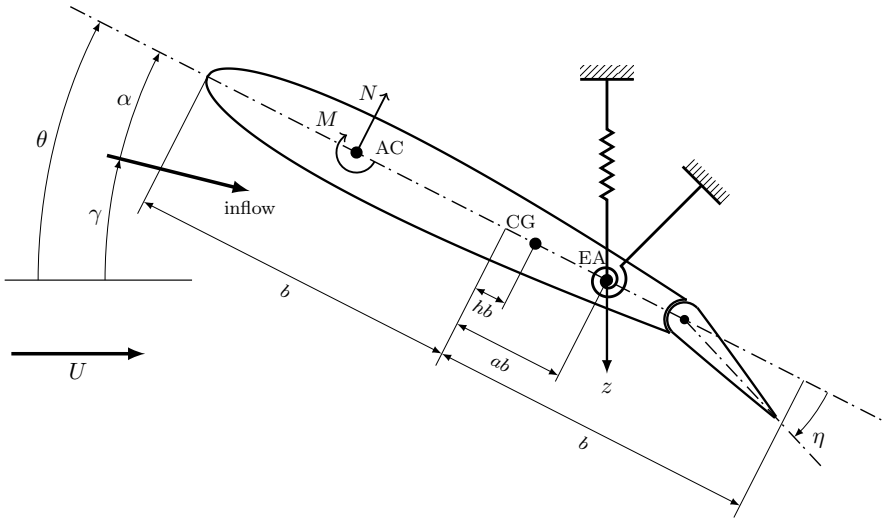

Fig. 1. Two-dimensional foil section.

point EA from the half-chord. The location of the center of gravity (CG) is defined by the dimensionless parameter h.

The elevator surface deflection is given by η, the pitch is θ and the pitch rate is given by $q = \dot{\theta}$. The plunge rate is $v = \dot{z}$ and the air-flow is horizontal with a speed U. The plunge rate and airflow combine to give an inflow at an angle γ with the horizontal. The resulting angle of attack (AoA) is given by $\alpha = \theta - \gamma$.

2.1 Aerodynamic Model

Assuming that for the attached flow condition the wing section aerodynamics model is linear, the normal force coefficient is given by

$$(C_{\mathrm{N}})_{\mathrm{lin}} = C_{\mathrm{N}_\alpha}\alpha + C_{\mathrm{N}_{\dot{\alpha}}}\dot{\alpha}\frac{2b}{U} + C_{\mathrm{N}_\eta}\eta \tag{1}$$

where C_{N_α}, $C_{\mathrm{N}_{\dot{\alpha}}}$, and C_{N_η} are constant derivatives quantifying the contributions from circulatory lift, impulsive loads, and the control surface respectively.

To model the separated flow condition, the relative position of the trailing-edge flow separation point along the chord is denoted by a non-dimensional state variable S which satisfies

$$\tau_1\dot{S} + S = \frac{1}{2}\left(1 - \tanh\left(\lambda_1(|\alpha - \tau_2\dot{\alpha}| - \alpha^*)\right)\right) \tag{2}$$

where the time constants τ_1 and τ_2 represent transient and quasi-steady aerodynamic effects respectively, λ_1 is a parameter that defines the static stall characteristics of the wing section and α^* represents the AoA corresponding to

$$S_0 = \frac{1}{2}\left(1 - \tanh\left(\lambda_1(|\alpha| - \alpha^*)\right)\right) = 0.5 \tag{3}$$

where S_0 is the separation point under static (steady-state) conditions [Pontillo et al., 2020].

As the trailing edge separation process evolves, the normal force coefficient is defined as

$$C_{\mathrm{N}} = (C_{\mathrm{N}})_{\mathrm{lin}}\big(1 - \delta(1 - S)\big) + C_{\mathrm{N}_S}(1 - S)k \tag{4}$$

where the parameter δ is the ratio of the loss to $(C_{\mathrm{N}})_{\mathrm{lin}}$, C_{N_S} is a constant parameter and k is the nonlinear aerodynamic factor defined as

$$k = \tanh\left(\lambda_2\alpha\right)\exp\left(-|\tau_4\dot{\alpha}|^n\right) \tag{5}$$

where the parameter λ_2 defines the range where the constant part decays, the time constant τ_4 defines the AoA rate condition and n is a shaping index. The quantity $\tanh\left(\lambda_2\alpha\right)$ captures the characteristics so that the constant C_{N_S} will dominate at high AoA and the term $\exp\left(-|\tau_4\dot{\alpha}|^n\right)$ allows the constant part to occur when AoA rate is low.

Under the attached flow condition, AC lies on the quarter chord, and it moves downstream as the separation progresses. The non-dimensional distance, G, of AC from the quarter chord with respect to the chord length is formulated as [Leishman and Beddoes, 1989]

$$\tau_3 \dot{G} + G = (1 - S_0)(G_S + G_\alpha |\alpha|) \tag{6}$$

where τ_3 defines the lag between G and AC displacement under steady conditions and G_S and G_α are coefficients to fit the AC displacement distribution in separation flow. Since the wing section is symmetric, it is assumed that the zero-lift moment is zero. The moment derivative of the control surface, C_{M_η}, can be assumed constant [Niel et al., 2017], then

$$C_{\mathrm{M}} = C_{\mathrm{N}} G + C_{\mathrm{M}_\eta} \eta \tag{7}$$

Defining $l = \frac{1}{2} + a$ as the relative distance between AC and EA, then it follows

$$M = 2\rho b^2 U^2 C_{\mathrm{M}} + lbN \tag{8}$$

where M is aerodynamic moment per unit wing span about the EA and N is the normal force per unit wing span defined as

$$N = \rho b U^2 C_{\mathrm{N}} \tag{9}$$

where ρ denotes the air density.

2.2 Full Aeroelastic Model

The equation of motion of a spring-restrained wing-section can be written as

$$\begin{bmatrix} m & mrb \\ mrb & I_{\mathrm{p}} \end{bmatrix} \begin{bmatrix} \dot{v} \\ \dot{q} \end{bmatrix} + \begin{bmatrix} c_z & 0 \\ 0 & c_\theta \end{bmatrix} \begin{bmatrix} v \\ q \end{bmatrix} + \begin{bmatrix} k_z & 0 \\ 0 & k_\theta \end{bmatrix} \begin{bmatrix} z \\ \theta \end{bmatrix} = \begin{bmatrix} -N\cos\theta \\ M \end{bmatrix} \tag{10}$$

where k_z and k_θ denote the translational and rotational stiffness coefficients respectively, c_z and c_θ denote the translational and rotational damping coefficients respectively, m and I_{p} denote the mass per unit wing span and the inertial per unit wing span about EA respectively, and the non-dimensional distance between EA and CG is defined as $r = a - h$.

The relationships between the kinematic and aerodynamic parameters are established as

$$\alpha = \theta + \arctan\frac{v}{U} \qquad\qquad \dot{\alpha} = q + \frac{\dot{v}U}{v^2 + U^2} \tag{11}$$

From the definitions of N and M given in (8) and (9)

$$\begin{aligned} \dot{v} &= f_v(z, v, \theta, q, S, G, U) \\ \dot{q} &= f_q(z, v, \theta, q, S, G, U) \end{aligned} \tag{12}$$

when $\eta = 0$. Define a state variable vector $\mathbf{x} = \begin{bmatrix} z, v, \theta, q \end{bmatrix}^{\mathrm{T}}$ and let the disturbance vector $\mathbf{d} = \begin{bmatrix} 1 - S, G \end{bmatrix}^{\mathrm{T}}$ capture the unknown state variables S and G. Then for a given U, (10) can be written as

$$\dot{\mathbf{x}} = \mathbf{f}(\mathbf{x}) + \mathbf{g}(\mathbf{x})\eta + \mathbf{e}(\mathbf{x}, t)\mathbf{d} \tag{13}$$

where $\mathbf{f} = \begin{bmatrix} v, f_v, q, f_q \end{bmatrix}^{\mathrm{T}}$, $\mathbf{g} = \begin{bmatrix} 0, g_v, 0, g_q \end{bmatrix}^{\mathrm{T}}$, $\mathbf{e} = \begin{bmatrix} 0, e_v, 0, e_q \end{bmatrix}^{\mathrm{T}}$. The variables g_v, g_q, e_v and e_q represent compatible vector functions.

Since $\mathbf{g}(\mathbf{x})$ is of full column rank, and without loss of generality the uncertainty term in (13) can be rewritten as $\mathbf{e}(\mathbf{x}, t)\mathbf{d} = \mathbf{g}(\mathbf{x})\xi + \tilde{\mathbf{e}}(\mathbf{x}, t)\tilde{\mathbf{d}}$, where $\tilde{\mathbf{e}}(\mathbf{x}, t)$ has the form of $\begin{bmatrix} 0, \tilde{e}_v, 0, 0 \end{bmatrix}^{\mathrm{T}}$. Since $\tilde{\mathbf{d}}$ does not affect the pitch rate, $\dot{\theta}$, directly, it can be simply ignored when designing the pitch angle reference tracking control. Therefore, (13) can be simplified as

$$\dot{\mathbf{x}} = \mathbf{f}(\mathbf{x}) + \mathbf{g}(\mathbf{x})\eta + \mathbf{g}(\mathbf{x})\xi \tag{14}$$

where $\xi \in \mathbb{R}$ is a scalar disturbance.

Now the problem is to ensure a stable and fast tracking control of the pitch angle of a foil section undergoing dynamic stall, which will be addressed in the next section.

3 Observer Based Sliding Mode Control

Consider a nonlinear state-dependent system as in (14) in the presence of external disturbance:

$$\begin{aligned}\dot{\mathbf{x}} &= \mathbf{f}(\mathbf{x}) + \mathbf{g}(\mathbf{x})\mathbf{u}_\mathrm{a} + \mathbf{g}(\mathbf{x})\xi \\ \dot{\mathbf{u}}_\mathrm{a} &= -(\boldsymbol{\Gamma} + \boldsymbol{\Delta})\mathbf{u}_\mathrm{a} + (\boldsymbol{\Gamma} + \boldsymbol{\Delta})\mathbf{u}\end{aligned} \tag{15}$$

where $\mathbf{x} \in \mathbb{R}^{n_x}$ is the plant state vector, $\mathbf{u}_\mathrm{a} \in \mathbb{R}^{n_u}$ is the actuator state vector, $\mathbf{u} \in \mathbb{R}^{n_u}$ is the system input vector, $\boldsymbol{\xi} \in \mathbb{R}^{n_u}$ is the external disturbance, $\mathbf{f}(\mathbf{x})$ and $\mathbf{g}(\mathbf{x})$ are known real functions of appropriate dimensions and they are assumed to be differentiable. In particular $\mathbf{g}(\mathbf{x})$ is supposed to be a full column matrix function. The diagonal matrix $\boldsymbol{\Gamma} \in \mathbb{R}_+^{n_u \times n_u}$ represents the known actuator time constants and the diagonal matrix $\boldsymbol{\Delta} \in \mathbb{R}^{n_u \times n_u}$ captures bounded uncertainties. Here it is assumed that $\boldsymbol{\Gamma} + \boldsymbol{\Delta}$ is positive definite and $\boldsymbol{\Delta}\boldsymbol{\Gamma}^{-1} \approx 0$. It is also assumed that $\boldsymbol{\xi}$ is differentiable and satisfies $\|\boldsymbol{\xi}\| \leq \bar{\xi}$ where the scalar $\bar{\xi}$ is known.

The following technical assumptions are required.

Assumption 1. *The system in* (15) *is stabilizable.*

Assumption 2. *The derivatives of the disturbance* $\boldsymbol{\xi}$ *are bounded and satisfy* $\lim_{t\to\infty} \left\|\dot{\boldsymbol{\xi}}\right\| = 0$.

Rearranging (15) yields

$$\begin{bmatrix}\dot{\mathbf{x}} \\ \dot{\mathbf{u}}_\mathrm{a}\end{bmatrix} = \begin{bmatrix}\mathbf{f}(\mathbf{x}) + \mathbf{g}(\mathbf{x})\mathbf{u}_\mathrm{a} \\ -\boldsymbol{\Gamma}\mathbf{u}_\mathrm{a}\end{bmatrix} + \begin{bmatrix}0 \\ \boldsymbol{\Gamma}\end{bmatrix}\mathbf{u} + \begin{bmatrix}\mathbf{g}(\mathbf{x}) \\ 0\end{bmatrix}\boldsymbol{\xi} + \begin{bmatrix}0 \\ \boldsymbol{\Delta}(-\mathbf{u}_\mathrm{a} + \mathbf{u})\end{bmatrix} \tag{16}$$

Due to the actuator dynamics, the disturbance $\boldsymbol{\xi}$ in (15) becomes 'unmatched' in (16) since the control input $\mathbf{u}$ does not appear in the input channel as $\boldsymbol{\xi}$.

In this paper, an NDO [Yang et al., 2013, Chen, 2003, 2004] is applied to estimate the unmatched disturbance $\boldsymbol{\xi}$ in (16)

$$\begin{aligned}\dot{\mathbf{s}} &= -\mathbf{w}(\mathbf{x})\mathbf{g}(\mathbf{x})\mathbf{s} - \mathbf{w}(\mathbf{x})\Big(\mathbf{g}(\mathbf{x})\mathbf{p}(\mathbf{x}) + \mathbf{f}(\mathbf{x}) + \mathbf{g}(\mathbf{x})\mathbf{u}_\mathrm{a}\Big) \\ \hat{\boldsymbol{\xi}} &= \mathbf{s} + \mathbf{p}(\mathbf{x})\end{aligned} \tag{17}$$

where $\mathbf{s} \in \mathbb{R}^{n_d}$ is the observer vector, $\mathbf{p}(\mathbf{x}) \in \mathbb{R}^{n_x} \to \mathbb{R}^{n_u}$ is a nonlinear function to be designed and $\hat{\boldsymbol{\xi}}$ represents the disturbance estimate. The observer gain $\mathbf{w}(\mathbf{x})$ is defined as

$$\mathbf{w}(\mathbf{x}) = \frac{\partial \mathbf{p}(\mathbf{x})}{\partial \mathbf{x}}. \tag{18}$$

Lemma 1. *[Chen, 2003] Under Assumption 2, the disturbance estimate* $\hat{\boldsymbol{\xi}}$ *of the NDO* (17) *can asymptotically track* $\boldsymbol{\xi}$ *of the system given by* (16) *if the observer gain* $\mathbf{w}(\mathbf{x})$ *is chosen such that for all* $\mathbf{x}$, $\mathbf{w}(\mathbf{x})\mathbf{g}(\mathbf{x})$ *is Hurwitz, which implies that the system*

$$\dot{\mathbf{e}}_\xi = -\mathbf{w}(\mathbf{x})\mathbf{g}(\mathbf{x})\mathbf{e}_\xi \tag{19}$$

is globally exponentially stable for all $\mathbf{x} \in \mathbb{R}^{n_x}$, *where* $\mathbf{e}_\xi = \boldsymbol{\xi} - \hat{\boldsymbol{\xi}}$ *is the estimation error.*

From Lemma 1, the disturbance estimation error $\mathbf{e}_\xi$ is bounded and satisfies

$$\mathbf{e}_\xi \leq \bar{\mathbf{e}}_\xi(t) = \bar{\mathbf{e}}_\xi(0)\mathrm{e}^{-t/\tau_e} \tag{20}$$

where $\bar{\mathbf{e}}_\xi(0)$ is a known itemwise-positive vector and τ_e is a time constant.

As in Yang et al. [2013], a sliding surface is developed for (16) in the presence of unmatched disturbances, given by:

$$\boldsymbol{\sigma} = \mathbf{K}\mathbf{x} + \mathbf{u}_\mathrm{a} + \hat{\boldsymbol{\xi}} \tag{21}$$

where $\boldsymbol{\sigma} \in \mathbb{R}^{n_u}$ is the switching function, $\mathbf{K} \in \mathbb{R}^{n_u \times n_x}$ is a controller gain matrix to be designed, and $\hat{\boldsymbol{\xi}}$ represents the disturbance estimate from Equation (17).

During sliding $\boldsymbol{\sigma} = \dot{\boldsymbol{\sigma}} = 0$, from (21) it follows $\mathbf{u}_\mathrm{a} = -\mathbf{K}\mathbf{x} - \hat{\boldsymbol{\xi}}$ and therefore

$$\dot{\mathbf{x}} = \mathbf{f}(\mathbf{x}) - \mathbf{g}(\mathbf{x})\mathbf{K}\mathbf{x} + \mathbf{g}(\mathbf{x})\mathbf{e}_\xi \tag{22}$$

Here it is assumed that $\mathbf{K}$ is selected to ensure the matrix $\mathbf{A}(\mathbf{x})$ is Hurwitz for all $\mathbf{x} \in \mathbb{R}^{n_x}$, where

$$\mathbf{A}(\mathbf{x}) = \frac{\partial \mathbf{f}(\mathbf{x})}{\partial \mathbf{x}} - \mathbf{g}(\mathbf{x})\mathbf{K} \tag{23}$$

which is possible under Assumption 1. Then the sliding motion is exponentially stable and subject to an exponentially decaying disturbance.

Remark 1. *The controller gain* $\mathbf{K}$ *can be calculated by rewriting the dynamic model*

$$\dot{\mathbf{x}} = \left(\frac{\partial \mathbf{f}(\mathbf{x})}{\partial \mathbf{x}} - \mathbf{g}(\mathbf{x})\mathbf{K} \right) \mathbf{x} \tag{24}$$

as a convex sum of linear ones, where nonlinearities are captured in functions that hold the convex sum property. The gain $\mathbf{K}$ *can be solved by solving a set of Linear Matrix Inequalities (LMIs) [Tapia et al., 2017].*

Define the NDO-based SMC law as

$$\mathbf{u} = -\mathbf{\Gamma}^{-1} \left(\mathbf{K} \left(\mathbf{f}(\mathbf{x}) + \mathbf{g}(\mathbf{x})\mathbf{u}_\mathrm{a} + \mathbf{g}(\mathbf{x})\hat{\boldsymbol{\xi}} \right) + \mathbf{\Gamma} \operatorname{sign} \boldsymbol{\sigma} \right) + \mathbf{u}_\mathrm{a} \tag{25}$$

where $\mathbf{\Gamma} \in \mathbb{R}^{n_u \times n_u}$ is a positive definite diagonal gain matrix to be designed.

Theorem 1. *Under Assumptions 1 and 2, the control law given by* (25) *will ensure a finite time convergence of* $\boldsymbol{\sigma}$ *if the observer gain* $\mathbf{w}(\mathbf{x})$*, and the gain* $\mathbf{\Gamma}$ *are designed as follows:*

- *the matrix* $-\mathbf{w}(\mathbf{x})\mathbf{g}(\mathbf{x})$ *is Hurwitz for all* $\mathbf{x} \in \mathbb{R}^{n_x}$*;*
- *for all* $\mathbf{x} \in \mathbb{R}^{n_x}$*, the following inequality holds:*

$$\lambda_{\min}(\mathbf{\Gamma}) \geq \left\| \left[\mathbf{K} + \mathbf{w}(\mathbf{x}) \right] \mathbf{g}(\mathbf{x}) \bar{\mathbf{e}}_\xi(0) \right\| + \eta_0, \tag{26}$$

where η_0 *is a small positive scalar and* $\lambda_{\min}(\mathbf{\Gamma})$ *represents the minimal eigenvalue of the real diagonal matrix* $\mathbf{\Gamma}$*.*

Proof. Define a Lyapunov candidate $V = \frac{1}{2}\boldsymbol{\sigma}^\mathrm{T}\boldsymbol{\sigma}$, then

$$\dot{V} = \boldsymbol{\sigma}^\mathrm{T}\dot{\boldsymbol{\sigma}} = \boldsymbol{\sigma}^\mathrm{T}(\mathbf{K}\dot{\mathbf{x}} + \dot{\mathbf{u}}_\mathrm{a} + \dot{\hat{\boldsymbol{\xi}}}) \tag{27}$$

From (16)–(18), it can be derived that

$$\dot{\hat{\boldsymbol{\xi}}} = \dot{\mathbf{s}} + \mathbf{w}(\mathbf{x})\dot{\mathbf{x}} = \mathbf{w}(\mathbf{x})\mathbf{g}(\mathbf{x})(\boldsymbol{\xi} - \hat{\boldsymbol{\xi}}) \tag{28}$$

Substituting (15) and (28) into (27) yields

$$\begin{aligned} \dot{V} &= \boldsymbol{\sigma}^\mathrm{T}(\mathbf{K}\big(\mathbf{f}(\mathbf{x}) + \mathbf{g}(\mathbf{x})\mathbf{u}_\mathrm{a} + \mathbf{g}(\mathbf{x})\boldsymbol{\xi}\big) \\ &\quad + (\mathbf{\Gamma} + \mathbf{\Delta})(-\mathbf{u}_\mathrm{a} + \mathbf{u}) + \mathbf{w}(\mathbf{x})\mathbf{g}(\mathbf{x})\mathbf{e}_\xi) \qquad (29) \\ &= \boldsymbol{\sigma}^\mathrm{T}(\mathbf{\Gamma}\mathbf{u} + \mathbf{K}(\mathbf{f}(\mathbf{x}) + \mathbf{g}(\mathbf{x})\mathbf{u}_\mathrm{a} + \mathbf{g}(\mathbf{x})\hat{\boldsymbol{\xi}}) \\ &\quad - \mathbf{\Gamma}\mathbf{u}_\mathrm{a} + \big(\mathbf{K} + \mathbf{w}(\mathbf{x})\big)\mathbf{g}(\mathbf{x})\mathbf{e}_\xi + \mathbf{\Delta}(-\mathbf{u}_\mathrm{a} + \mathbf{u})) \qquad (30) \end{aligned}$$

Substituting the control law in (25) into (29) and using the fact that $\mathbf{\Delta}\mathbf{\Gamma}^{-1} \approx 0$, (29) can be written as

$$\begin{aligned} \dot{V} &\approx \boldsymbol{\sigma}^\mathrm{T}(-\mathbf{\Gamma} \operatorname{sign} \boldsymbol{\sigma} + \big(\mathbf{K} + \mathbf{w}(\mathbf{x})\big)\mathbf{g}(\mathbf{x})\mathbf{e}_\xi) \qquad (31) \\ &\leq -\lambda_{\min}(\mathbf{\Gamma}) \left\| \boldsymbol{\sigma} \right\| + \left\| \boldsymbol{\sigma} \right\| \left\| \big(\mathbf{K} + \mathbf{w}(\mathbf{x})\big)\mathbf{g}(\mathbf{x}) \right\| \left\| \mathbf{e}_\xi \right\| \qquad (32) \end{aligned}$$

Using (20) it follows

$$\dot{V} \leq -\lambda_{\min}(\mathbf{\Gamma}) \left\| \boldsymbol{\sigma} \right\| + \left\| \boldsymbol{\sigma} \right\| \left\| \big(\mathbf{K} + \mathbf{w}(\mathbf{x})\big)\mathbf{g}(\mathbf{x}) \right\| \bar{\mathbf{e}}_\xi(0) \tag{33}$$

By selecting the modulation gain as (26)

$$\dot{V} \leq -\eta_0 \left\| \boldsymbol{\sigma} \right\| = -\eta_0 V^{1/2} \tag{34}$$

and therefore $\boldsymbol{\sigma} \to 0$ in finite time. □

4 Simulation and Results

4.1 Aerodynamic model simulation

Simulation results associated with the proposed revised aerodynamics model of the NACA 0012 airfoil are presented here. The experimental data and the conventional L/B model representations are taken from Sánchez Martínez et al. [2019].

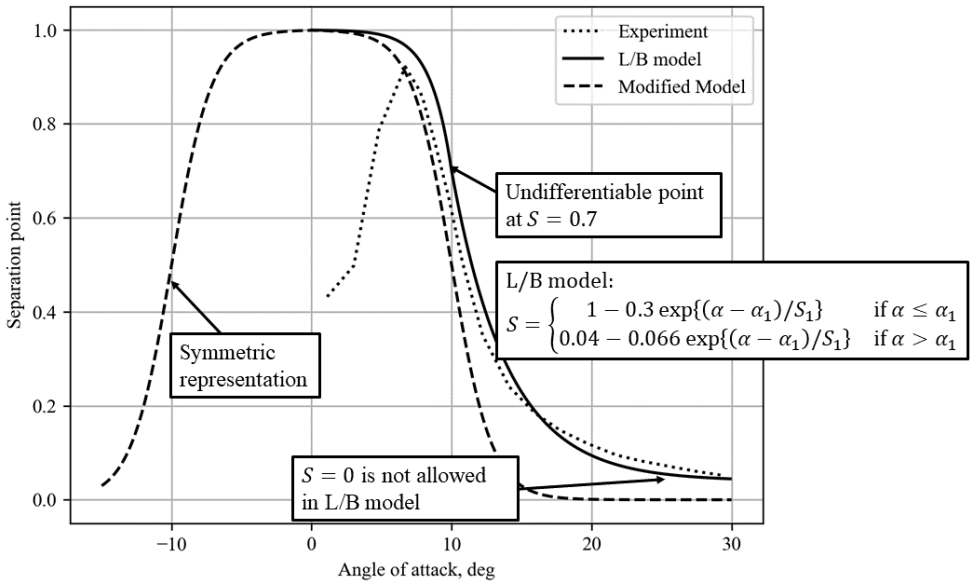

Fig. 2. Comparison between separation point distribution in static stall experiments and its representations from L/B model and the revised model.

Fig. 2 shows a comparison between the predictions of the conventional L/B model (solid line), the modified model proposed in this paper (dashed line) and one from the experimental data (dotted line). Compared to the piece-wise approximation of the conventional L/B model [Leishman and Beddoes, 1989], the proposed model is continuous.

There are two major differences between the estimates from the proposed model and the experimental data. In the low AoA region, the laminar separation bubble near the leading edge [Leishman and Beddoes, 1989] is ignored in both the conventional L/B model and the revised model, since it is trailing edge separation that plays a significant role in the onset of dynamic stall [Leishman and Beddoes, 1989]. The discrepancy in the high AOA region is caused by inaccuracy of the experimental data, because the separation point cannot be measured directly in experiments, but is usually calculated by inverting the relation of normal force to separation point defined in the conventional L/B model.

Note that the conventional L/B model does not allow S to be less than 0.04, which restricts the prediction performance at high AoA, while the revised model does not have this restriction. Fig. 2 also shows the symmetric representation of the proposed model.

The normal force coefficient variations in static (solid and dashed lines) and dynamic stall (dash-dotted and dotted lines) are plotted in Fig. 3. In the dynamic stall experiment, the normal force has a large overshoot before detachment occurs because of the large hysteresis of the separation point. Then it falls to the value that matches the static stall experiment data as the AoA increases to its maximal value in the oscillation period. The proposed model explains this by the fact that the nonlinear factor given by (5) is large since the AoA rate is small and the flow is separated with high AoA, so the C_{N_S} term in (4) dominates. However, when the wing section is pitching down, the normal force drops more than in static stall, because as the AoA rate goes up, the weight on C_{N_S} decays. Finally, in the reattachment process, no overshoot is observed, because the effect of C_{N_S} disappears at low AoA.

Clearly from Fig. 4, the proposed model has better predictions. These show that the L/B model fails to consider the constant part so that its static normal force estimate is not accurate at high AoA [Boutet et al., 2020].

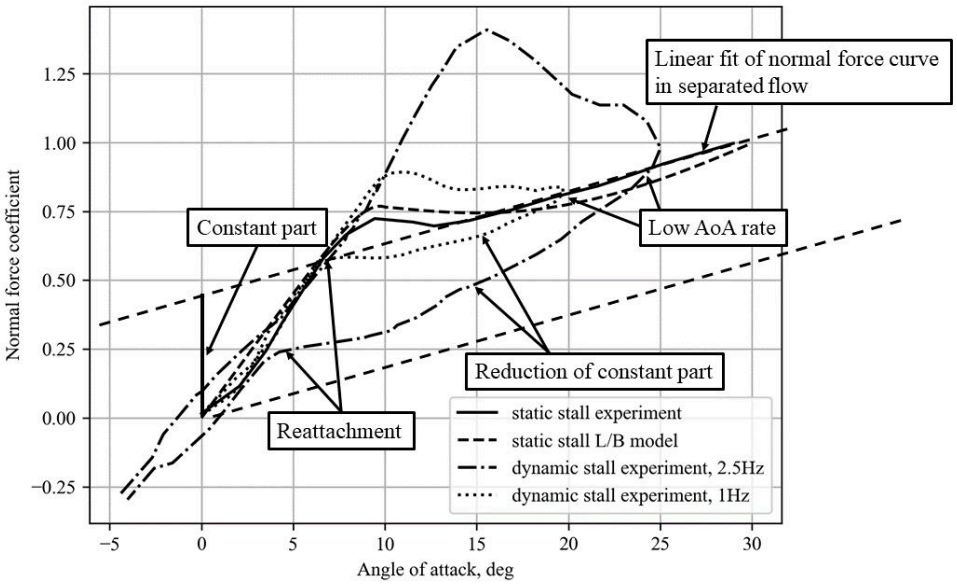

Fig. 3. Comparison between normal force coefficient distribution in static stall experiment and dynamic stall experiment.

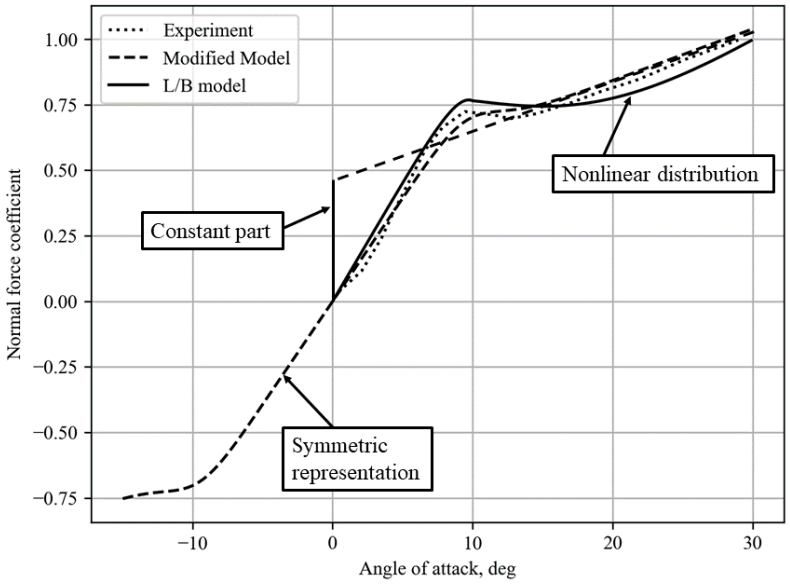

Fig. 4. Comparison between normal force coefficient distribution in static stall experiment and its representations from the L/B model and the revised model.

Figures 5a and 5b show the normal force distributions in dynamic stall with frequencies of 2.5 Hz and 1 Hz. Both the revised model and the L/B model delay the time when C_N reaches its peak. In the conventional L/B model prediction, there is an unexpected notch in the detachment procedure marked as "unwanted dynamics" on the plots. This results from the undifferentiable point of the static S-fitting. Data consistency was verified by measuring the $\mathcal{L}_2$-norm of error between estimates and experiment data listed in Table 1, which shows that the revised model provides better estimation

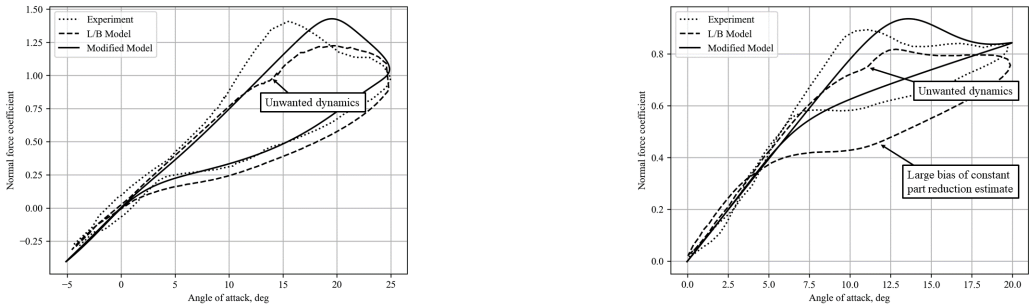

(a) Frequency of 2.5 Hz

(b) Frequency of 1 Hz

Fig. 5. Comparison between normal force coefficient distribution in dynamics stall experiment and its representations from the L/B model and the revised model.

for C_{N}.

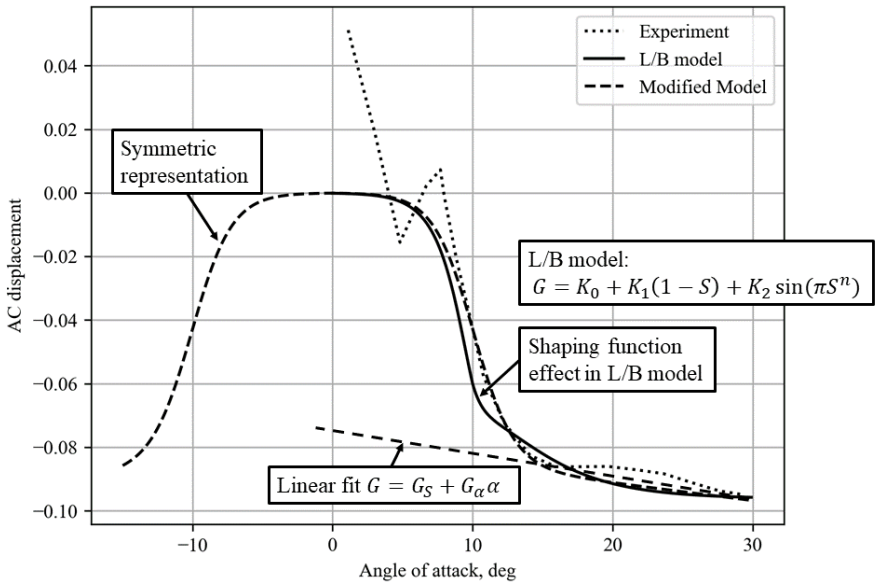

Fig. 6. Comparison of AC displacement distribution in static stall experiment and its representations from the L/B model and the revised model.

The representation of AC displacement given by the revised model, compared with that given by the conventional L/B model, is shown in Fig. 6. Similarly, the mismatch in the low AoA region results from ignorance of the leading edge laminar bubble. Apart from this, the prediction from the proposed model is generally better the that from the conventional L/B model. The moment coefficient with respect to the quarter chord changes during the separation process due to AC displacement, as illustrated in Fig. 7. Both model predictions match the experimental data well.

Fig. 8 clearly illustrates the time lag of the AC displacement, which is much shorter than that of the separation point. This implies that G is not a function of S as Leishman and Beddoes [1989] suggest. There must be an independent state variable to represent the time lag. Although the conventional L/B model has excellent prediction for static moment coefficient, Figures 9a and 9b show that the performance of the conventional L/B model for dynamic moment coefficient prediction is poor, whereas the revised model gives much better results. An error comparison is also listed in Table 1.

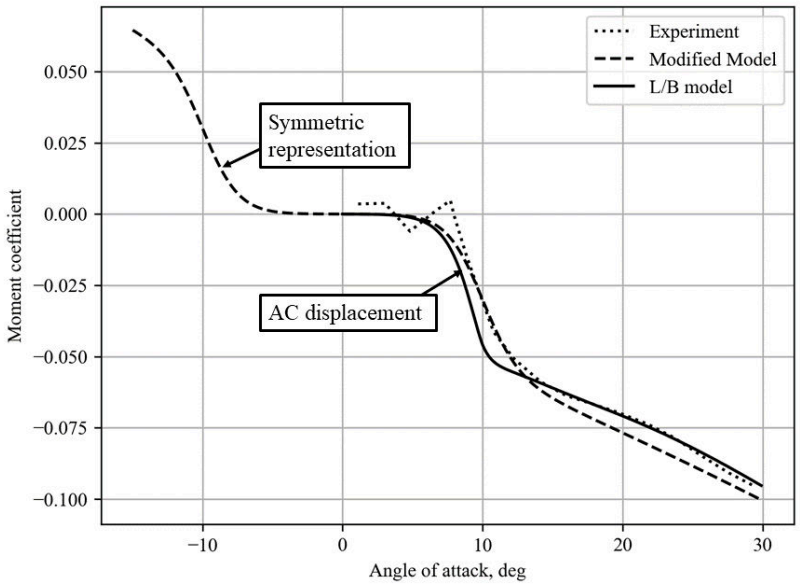

Fig. 7. Comparison between moment coefficient distribution in static stall experiment and its representations from the L/B model and the revised model.

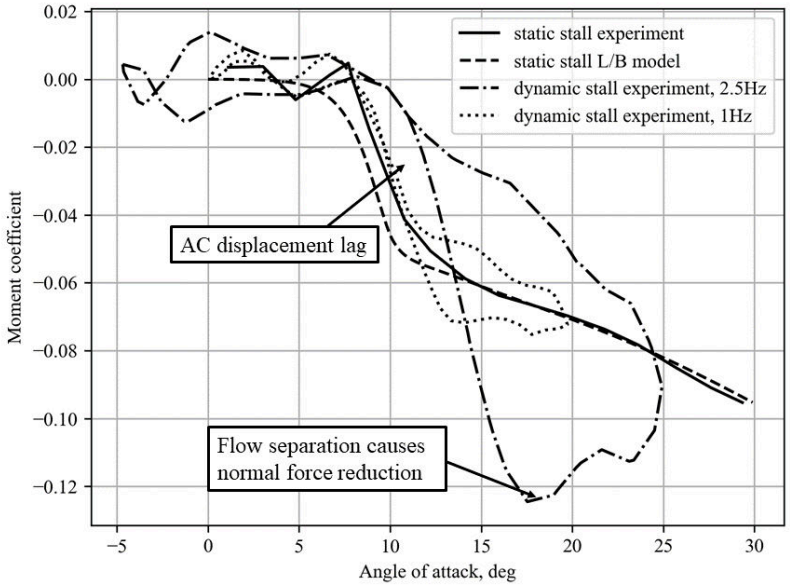

Fig. 8. Comparison between moment coefficient distribution in static stall experiment and dynamic stall experiment.

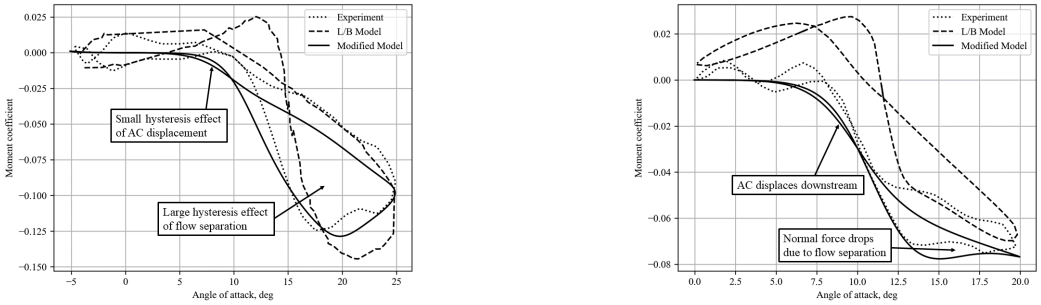

(a) Frequency of 2.5 Hz

(b) Frequency of 1 Hz

Fig. 9. Comparison between moment coefficient distribution in dynamics stall experiment and its representations from the L/B model and the revised model.

Item	Setting (Hz)	Revised model	L/B model
C_{N}	2.5a	0.148	0.242
C_{N}	2.5b	0.068	0.124
C_{M}	2.5a	0.135	0.442
C_{M}	2.5b	0.217	0.141
C_{N}	1.0a	0.103	0.153
C_{N}	1.0b	0.111	0.276
C_{M}	1.0a	0.094	0.606
C_{M}	1.0b	0.180	0.426

Table 1. The $\mathcal{L}_2$-norm errors between predictions from different models and experiment results. In the "setting" column, the number indicates the frequency (Hz) of dynamic stall; the character "a" represents increasing AoA, whereas "b" decreasing AoA.

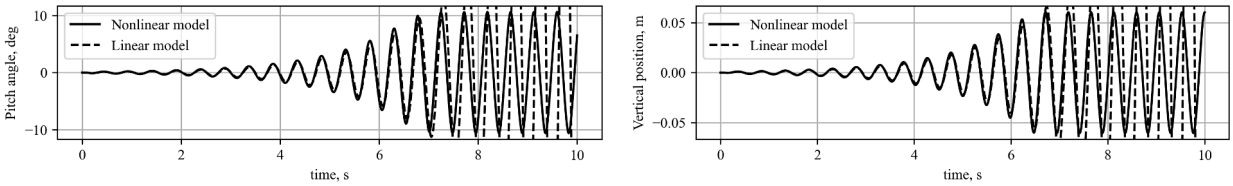

(a) Pitch response

(b) Plunge response

Fig. 10. Aeroelastic responses to small disturbance.

4.2 Open-loop Simulation

This subsection investigates the aeroelastic response undergoing stall flutter with respect to the incoming flow speed. The model parameters are given in Table 2. The half-chord, b, is from Sánchez Martínez et al. [2019] and the air density ρ is taken at sea-level. The mass and inertia parameters are assumed.

The static aerodynamic parameters, C_{N_α}, δ and α^* are tuned so that the static stall matches the experimental data. Similarly, the dynamic aerodynamic derivatives, $C_{\mathrm{N}_{\dot{\alpha}}}$ and C_{N_S}, and the dynamic model parameters λ_1, λ_2, n, τ_1, τ_2, τ_3 and τ_4 are tuned so that the dynamic stall matches the experimental data. The elevator aerodynamic coefficients, C_{N_η} and C_{M_η}, are assumed based on the geometry. The aerodynamic centre model parameters, G_S and G_α are obtained by fitting the AC displacement. The aeroelastic parameters k_z, k_θ, c_z and c_θ are tuned to yield a stall flutter at speed of $7.5\,\mathrm{m\,s^{-1}}$ to match that of Martinez's experiment [Sánchez Martínez et al., 2019], as are the CG and EA centers, h and a. Some further details are given in **?**.

Parameter	Value	Parameter	Value
C_{N_α}	4.50	$C_{\mathrm{N}_{\dot{\alpha}}}$	0.41
C_{N_η}	0.90	C_{N_S}	0.45
δ	0.75	C_{M_η}	-0.45
λ_1	20	λ_2	10
α^*	$\pi/18$ rad	n	4
G_S	-0.08	G_α	-0.032
τ_1	0.025 s	τ_2	0.051 s
τ_3	0.005 s	τ_4	0.25 s
m	$0.077\,\mathrm{kg\,m^{-1}}$	I_p	$2.3\times10^{-4}\,\mathrm{kg\,m}$
b	0.019 m	ρ	$1.225\,\mathrm{kg\,m^{-3}}$
h	0.167	a	0.167
k_z	$3.85\,\mathrm{N\,m^{-2}}$	k_θ	$0.069\,\mathrm{N\,rad^{-1}}$
c_z	$0.0038\,\mathrm{N\,s\,m^{-2}}$	c_θ	$0.0023\,\mathrm{N\,s\,rad^{-1}}$

Table 2. Wing-section model parameters

Apart from the equilibrium at zero AoA resulting from the symmetry of the wing-section, all other static equilibrium points are functions of incoming flow speed U by letting $\dot{z} \equiv 0$, which implies $\alpha = \theta$. The static solutions of the equilibrium implies that the critical air speed is about 6.74 m/s. With a larger air speed, the open loop system becomes unstable. At a speed of about 7.24 m/s, the unstable mode becomes significant.

The aeroelastic responses at a flow speed of $U = 7.5$ m/s are exemplified in Fig. 10 to show that LCOs will result following a perturbation. A small doublet input with amplitude of 0.01 rad and time interval of 0.1 s is used as the input excitation. The pitch and plunge responses are shown in Fig. 10, where it can be seen that the nonlinear model response deviates from the linear model after the dynamic stall commences.

4.3 Closed-loop Simulation

In this subsection, the closed-loop simulation results are presented to show the effectiveness of the observer based controller. The controller proposed in Section 3 is applied to the model. Assumption 1 is easily checked from the

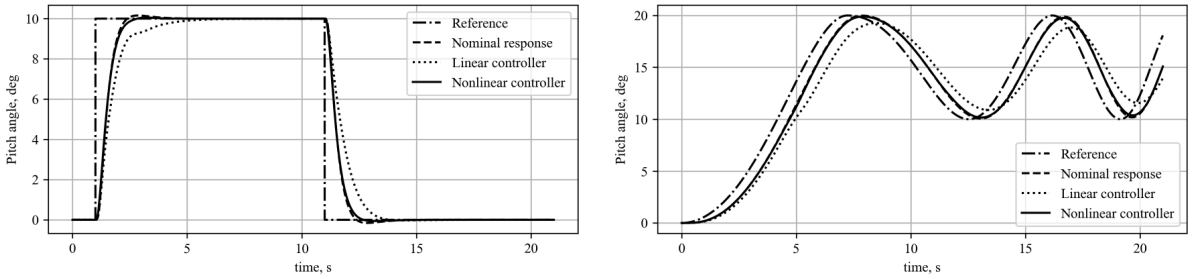

(a) Closed-loop response to bi-directional step reference **(b)** Closed-loop response to time-varying reference

Fig. 11. Closed-loop responses at speed of 6.8 m/s.

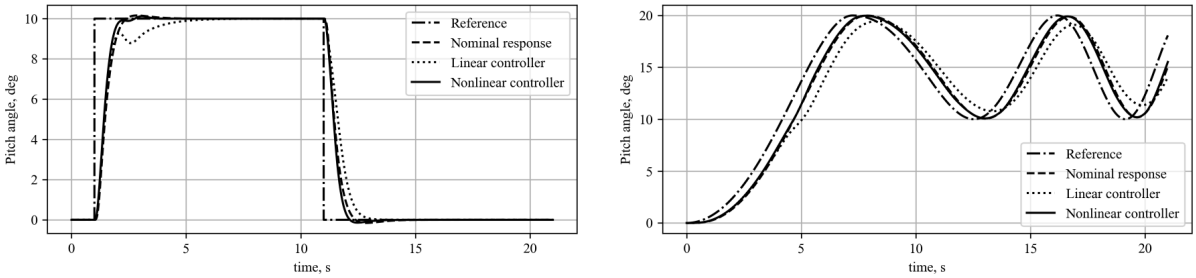

(a) Closed-loop response to bi-directional step reference **(b)** Closed-loop response to time-varying reference

Fig. 12. Closed-loop responses at speed of 7.5 m/s.

model. Since the control surface generates pitch moment, state variable q and hence θ can be controlled. Because the lift is dependent on θ, state variable w and hence z are also controllable and the system is thus stabilizable. Assumption 2 is satisfied because the disturbance, ξ, is introduced by flow separation in dynamic stall, so that the bound of ξ is limited by the aerodynamics. As the system is stabilized, the separation point is fixed and the disturbance becomes constant, which means $\dot{\xi}$ approaches zero.

Simulation results associated with flow speeds of 6.8 m/s, 7.5 m/s, 8.5 m/s are shown in Figures 11, 12, and 13 respectively. The control signals at the 7.5 m/s flow speed are shown in Fig. 14. In addition, a simulation response for a large flow speed of 9.5 m/s is shown in Fig. 15.

The controller gain matrix $\mathbf{K} \in \mathbb{R}^5$ is designed as

$$\mathbf{K} = \begin{bmatrix} 0.6731 & -0.8279 & -6.7351 & -0.9515 & 17.3205 \end{bmatrix} \tag{35}$$

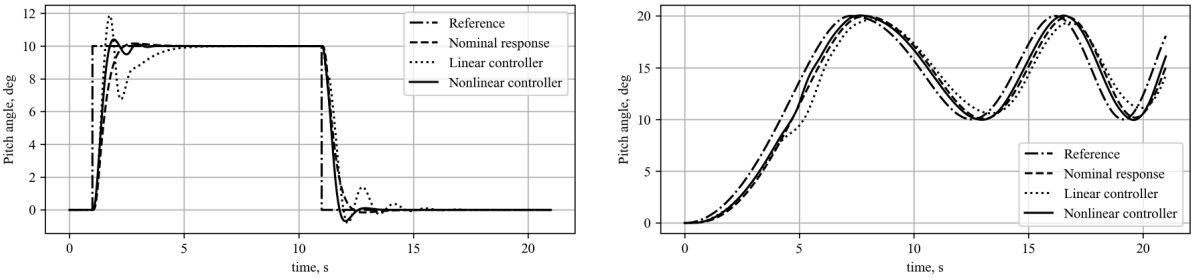

(a) Closed-loop response to bi-directional step reference **(b)** Closed-loop response to time-varying reference

Fig. 13. Closed-loop responses at speed of 8.5 m/s.

The observer nonlinear function is given by:

$$p(x) = -z - v - \theta - q \tag{36}$$

and the gain $\mathbf{\Gamma} = 5$. Assume that the time constant of the actuator is approximately 0.1 s, then $\mathbf{\Gamma} = 10$. The uncertainty $\mathbf{\Delta}$ is 10% of $\mathbf{\Gamma}$.

To demonstrate the effectiveness of the proposed control scheme, a nominal closed-loop performance, generated by applying a linear control law to a model linearised at zero AoA, is introduced here. Furthermore the linear feedback control is applied to the full nonlinear model and its closed-loop responses, labelled "Linear controller" in the following figures, are also used for comparison.

As can be seen from Figures 11 to 13, the proposed control scheme (labelled "Nonlinear controller") achieves a performance close to the nominal, and is much better than the response of the nonlinear model under the linear controller with large unmatched disturbances resulting from the dynamic stall (as the AoA approaches 9°) and from the actuator dynamics.

Figure 14 shows the control effector demand and elevator responses with a flow speed of 7.5 m/s. The effect of the actuator lag dynamics, modelled by a first order lag, can be seen. It should be noted that the elevator deflection for the time-varying reference, shown in Figure 14b, is infeasibly large. Elevator deflections are typically restricted to a maximum magnitude of about 20°, this is significantly exceeded. Thus, in practice, the elevator requires resizing to cope with the large pitch angle requirements of the reference.

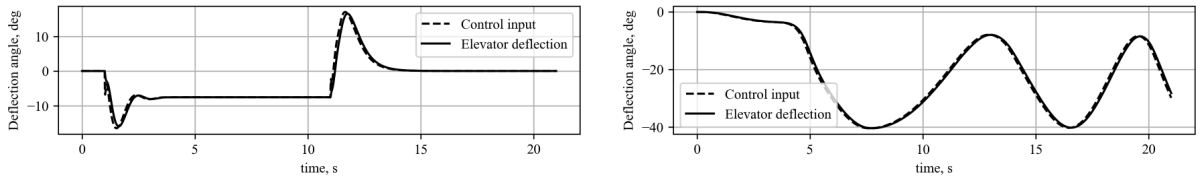

(a) Closed-loop control signal for bi-directional step reference **(b)** Closed-loop control signal for time-varying reference

Fig. 14. Closed-loop control signal at speed of 7.5 m/s.

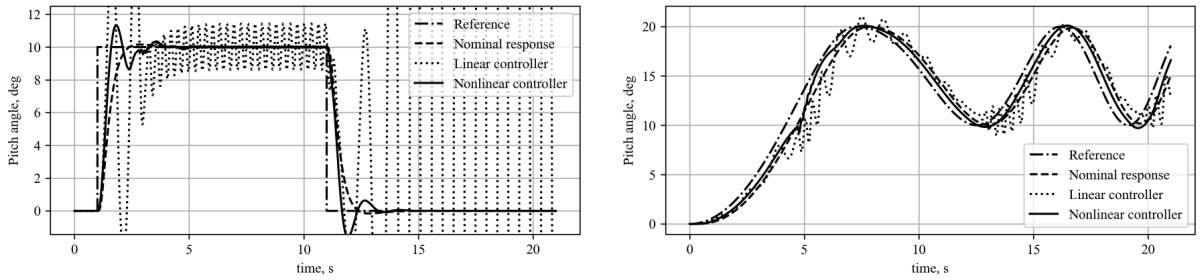

(a) Closed-loop response to bi-directional step reference **(b)** Closed-loop response to time-varying reference

Fig. 15. Closed-loop responses at speed of 9.5 m/s.

When the flow speed is 9.5 m/s, as can be seen from Fig. 15, the linear controller cannot ensure stability and large oscillations appear. The performance of the proposed controller under the attached flow condition is also shown in Fig. 15. The results are good and show that the amplitude and frequency of oscillations are successfully suppressed.

The simulation results and analysis demonstrate that the controller proposed in this paper is able to suppress stall flutter and obtain a fast, stable, and robust reference tracking for pitch angle.

5 Conclusion

In this paper, an aeroelastic model for stall flutter of a two-dimensional wing-section was developed and a nonlinear disturbance observer based sliding mode controller was developed as a solution of the active flutter suppression

problem. The novel stall flutter model improved the modelling of a two-dimensional wing section aeroelastics with small Reynolds number and Mach number. The disturbance observer based sliding mode controller is capable of mitigating the degradation of the performance caused by unmatched disturbances. Simulation results show the efficacy of the method and good pitch tracking performance was ensured.

The work has several limitations. The model has not been validated beyond the data in the references. Improvements to the aeroelastic model are required and various wing-section scales and flow conditions considered. In particular, the aerodynamics of the elevator have not been accurately modelled, and the elevator size is not large enough to achieve the time varying reference demand. Wind tunnel tests to determine the elevator aerodynamic coefficients and non-linear flow effects are required for future work. Implementation in a wind tunnel of the closed-loop scheme is also needed to validate the controller.

Data Availability Statement

Some or all data, models, or code that support the findings of this study are available from the corresponding author upon reasonable request.

Acknowledgments

Financial support from the program of China Scholarships Council (CSC) is acknowledged.

References

J. Beedy, G. Barakos, K. J. Badcock, and B. E. Richards. Non-linear analysis of stall flutter based on the ONERA aerodynamic model. *Aeronautical Journal*, 107(1074):495–509, 2003. ISSN 00019240. doi: 10.1017/S0001924000134001.

D. Borglund and J. Kuttenkuler. Active wing flutter suppression using a trailing edge flap. *Journal of Fluids and Structures*, 16:271–294, 2002. doi: 10.1006/jfls.2001.0426.

Johan Boutet, Grigorios Dimitriadis, and Xavier Amandolese. A modified Leishman–Beddoes model for airfoil sections undergoing dynamic stall at low Reynolds numbers. *Journal of Fluids and Structures*, 93:102852, 2020. ISSN 10958622. doi: 10.1016/j.jfluidstructs.2019.102852.

Wen-Hua Chen. Nonlinear disturbance observer-enhanced dynamic inversion control of missiles. *Journal of Guidance, Control, and Dynamics*, 26(1):161–166, 2003. doi: 10.2514/2.5027.

Wen Hua Chen. Disturbance observer based control for nonlinear systems. *IEEE/ASME Transactions on Mechatronics*, 9(4):706–710, 2004. ISSN 10834435. doi: 10.1109/TMECH.2004.839034.

Jr. Doggett, R. V. and J. L. Townsend. Flutter suppression by active control and its benefits. In *Proceedings of the SCAR Conference*, volume 1 of *NASA Conference Publication*, pages 303–335, Hampton, VA, November 1976.

Christopher Edwards and S Spurgeon. *Sliding Mode Control*. CRC Press, 1998. ISBN 9780429075933. doi: 10.1201/9781498701822.

Casey Fagley, Jurgen Seidel, and Thomas McLaughlin. Experimental investigation of the aeroelastic behavior of a NACA0018 cyber-physical flexible wing. In *AIAA Applied Aerodynamics Conference*, pages 22–26, Dallas, TX, 2015. doi: 10.2514/6.2015-2251.

J. G. Leishman and T. S. Beddoes. A semi-empirical model for dynamic stall. *Journal of the American Helicopter Society*, 34(3):3–17, 1989. ISSN 00028711. doi: 10.4050/JAHS.34.3.

Nailu Li, Mark J. Balas, Pourya Nikoueeyan, Hua Yang, and Jonathan W. Naughton. Stall flutter control of a smart blade section undergoing asymmetric limit oscillations. *Shock and Vibration*, 2016(Article ID 5096128), 2016. ISSN 10709622. doi: 10.1155/2016/5096128.

E. Livne. Aircraft active flutter suppression: State of the art and technology maturation needs. *Journal of Aircraft*, 55 (1):410–452, 2018. doi: 10.2514/1.C034442.

Tamás Luspay, Tamás Baár, Dániel Teubl, Bálint Vanek, Daniel Ossmann, Matthias Wüstenhagen, Manuel Pusch, Thiemo Kier, Sérgio Waitman, Andrea Iannelli, Andres Marcos, and Mark Lowenberg. Flight control design for a highly flexible flutter demonstrator. In *AIAA Scitech 2019 Forum*, number AIAA 2019-1817, 2019. doi: 10.2514/6.2019-1817.

Fabien Niel, Alexandre Seuret, Luca Zaccarian, and Casey Fagley. Robust LQR control for stall flutter suppression: A polytopic approach. *IFAC-PapersOnLine*, 50(1):11367–11372, 2017. doi: 10.1016/j.ifacol.2017.08.2041.

J. Peiró, U. Galvanetto, and C. Chantharasenawong. Assessment of added mass effects on flutter boundaries using the Leishman-Beddoes dynamic stall model. *Journal of Fluids and Structures*, 26(5):814–840, 2010. doi: 10.1016/j.jfluidstructs.2010.04.002.

Alessandro Pontillo, Sezsy Yusuf, Guillermo Lopez, Dominic Rennie, and Mudassir Lone. Investigating pitching moment stall through dynamic wind tunnel test. *Proceedings of the Institution of Mechanical Engineers, Part G: Journal of Aerospace Engineering*, 234(2):267–279, 2020. doi: 10.1177/0954410019861853.

N. Ramos-Pedroza, W. MacKunis, and M. Reyhanoglu. A sliding mode LCO regulation strategy for dual-parallel underactuated UAV systems using synthetic jet actuators. *International Journal of Aerospace Engineering*, 2015 (Article ID 795348), 2015. doi: 10.1155/2015/795348.

Mariano Sánchez Martínez, Johan Boutet, Xavier Amandolese, Vincent Terrapon, and Grigorios Dimitriadis. Computation of Leishman-Beddoes model parameters using unsteady RANS simulations. In *AIAA Scitech 2019 Forum*, number AIAA 2019-1854, 2019. doi: 10.2514/6.2019-1854.

W. Sheng, R. A.Mc D. Galbraith, and F. N. Coton. A new stall-onset criterion for low speed dynamic-stall. *Journal of Solar Energy Engineering*, 128(4):461–471, 2006. doi: 10.1115/1.2346703.

Zhiwei Sun, Sohrab Haghighat, Hugh H.T. Liu, and Junqiang Bai. Time-domain modeling and control of a wing-section stall flutter. *Journal of Sound and Vibration*, 340:221–238, 2015. ISSN 10958568. doi: 10.1016/j.jsv.2014.10.028.

Béla Takarics, Bálint Patartics, Tamás Luspay, Péter Bauer, Bálint Vanek, Christian Rößler, Julius Bartasevicius, Sebastian Köberle, Daniel Teubl, Mirko Hornung, Sergio Waitman, Andres Marcos, Manuel Pusch, Matthias Wüstenhagen, Thiemo Kier, Gertjan Looye, and Yasser M. Meddaikar. Active flutter mitigation testing on the FLEXOP demonstrator aircraft. In *AIAA Scitech 2020 Forum*, number AIAA 2020-1970, 2020. doi: 10.2514/6.2020-1970.

Alán Tapia, Miguel Bernal, and Leonid Fridman. Nonlinear sliding mode control design: An LMI approach. *Systems and Control Letters*, 104:38–44, 2017. ISSN 01676911. doi: 10.1016/j.sysconle.2017.03.011.

Julian Theis, Harald Pfifer, and Peter J. Seiler. Robust Control Design for Active Flutter Suppression. In *AIAA Atmospheric Flight Mechanics Conference*, number AIAA 2016-1751, Reston, VA, 2016. doi: 10.2514/6.2016-1751.

V. I. Utkin. *Sliding Modes in Control and Optimization*. Springer, Berlin, Germany, 1992. doi: 10.1109/TAC.1977.1101446.

M. R. Waszak and S. Srinathkumar. Flutter suppression for the active flexible wing: A classical design. *Journal of Aircraft*, 32(1):61–67, 1995. ISSN 00218669. doi: 10.2514/3.46684.

Chao Yang, Chen Song, Zhigang Wu, and Changchuan Xie. Application of output feedback sliding mode control to active flutter suppression of two-dimensional airfoil. *Science China Technological Sciences*, 53(5):1338–1348, 2010. ISSN 16747321. doi: 10.1007/s11431-010-0099-z.

Jun Yang, Shihua Li, and Xinghuo Yu. Sliding-mode control for systems with mismatched uncertainties via a disturbance observer. *IEEE Transactions on Industrial Electronics*, 60(1):160–169, 2013. ISSN 02780046. doi: 10.1109/TIE.2012.2183841.

Active stall flutter suppression for a revised Leishman/Beddoes model

Zheng, Junruoyu

2024-01-01

Zheng J, Pontillo A, Chen L, Whidborne JF, (2024) Active stall flutter suppression for a revised Leishman/Beddoes model. Journal of Aerospace Engineering, Volume 37, Issue 1, January 2024 https://doi.org/10.1061/JAEEEZ.ASENG-5003